Electromagnetic Energy Density in Dispersive and Dissipative Media

Frederico Dias Nunes

Thiago Campos Vasconcelos

Marcel Bezerra

Grupo de Engenharia da Informacao, DES,CP.7.800
Recife-SP, CEP50670-000,UFPE
and IFSC-INSC, USP, CP, 369, Sao Carlos-SP, CEP 13560-970, Brazil
fdnunes@ufpe.br

John Weiner

Center for Nanoscale Science and Technology, National Institute of Standards and Technology, 100 Bureau Drive, Stop 6203, Gaithersburg, MD 20899-6203, USA
and IFSC-INOF,USP, CP, 369, Sao Carlos-SP, CEP 13560-970, Brasil
jweiner@nist.gov

Abstract

The description of the energy density associated with an electromagnetic field propagating through matter must treat two different phenomena: dispersion, the variation of the refractive index with frequency, and dissipation, the loss of field energy by absorption. In many cases, as in common dielectrics, the dispersive medium is essentially transparent so dissipation can be neglected. For metals, however, both dispersion and dissipation must be taken into account, and their respective contributions vary significantly with the frequency of the electromagnetic field. Plasmonic structures such as slits, holes and channel waveguides always involve surfaces between dielectrics and metals, and the energy density in the vicinity of the interface figures importantly in the dynamic response of these structures to light excitation in the visible and near-infrared spectral regions. Here we consider the electromagnetic energy density propagated on and dissipated at real metal-dielectric surfaces, including the important SPP, the surface plasmon-polariton wave guided by the interface. We show how the "stored energy" oscillates over an optical cycle between the plasmonic structure and the propagating surface mode, while the dissipated energy continues to accumulate over the same period. We calculate these energy densities for the case of the silver-air interface (using two data sets for silver permittivity commonly cited in the research literature) over a range of frequencies corresponding to the range of wavelengths from 200 to 2000nm.

OCIS codes: 240.6680,240.690,260.2110,260.3910,310.6628

1. Introduction

The field of "nanoplasmonics," the study of the electromagnetic response of subwavelength-scaled conductive objects embedded in a dielectric media, is leading to new discoveries and insights into the basic physics of these phenomena as well as opening new technologies for molecular and environmental sensing [1], information storage [2], high-speed and wide-band communications [3], solar energy conversion [4], and even the possibility of a new paradigm in circuit functionality based on displacement current switching in metamaterials rather than free charge current switching that underlies conventional complementary metal-oxide semiconductor (CMOS) technology [5]. The common feature running through all these pursuits is the spatial localization of electromagnetic energy well below the optical diffraction limit at wavelengths ranging from the visible to the near infrared. This energy can take the form of propagating surface waves or resonant standing-wave modes at specific positions on the periphery of subwavelength-scale conductive objects. In both cases the energy density of the field increases discontinuously, usually by many-fold, at the dielectric-conductor interface.

In addition to nanoplasmonics as described above another related burgeoning field, "metamaterials," is attracting a great deal of interest. The focus in metamaterials is to fashion the optical response of fabricated, composite subwavelength structures in periodic arrays so as to achieve polarization and magnetization properties not found in naturally occurring materials. Structured arrays combining subwavelength-scale wires and split-ring resonators, for example, can exhibit negative permittivity and permeability within a particular frequency range, thus giving rise to negative index of refraction and other unusual optical properties [6]. Alternating slabs of dielectric and metal, each with subwavelegth thickness, provides another example of a metamaterial exhibiting negative permittivity and permeability within the same frequency interval [7]. The proper characterization of energy density, including stored energy and dissipative energy, in metamaterials where the permittivity and permeability both exhibit strong dispersion and loss has stimulated a flurry of recent studies [8–10], and a recent publication has even proposed that negative energy density may have a real physical meaning [11].

Metamaterials are usually some periodic array of subwavelength structures exhibiting capacitive and inductive electric and magnetic properties. However, another class of important subwavelength arrays consist of metal-insultaor-metal (MIM) channels [12] and networks of these channels, recently termed "resonant guided wave networks" (RGWNs) [13]. The optical response of these waveguides does not include significant magnetization, but they do exhibit frequency dispersion in a lossy medium. It is therefore worthwhile to obtain reliable dispersion expressions for the stored and dissipative energy density in these structures. We study here the behavior of the energy density at the interface where dispersion, dissipation, and phase response are governed by the behavior of the complex permittivity and conductivity

of the adjacent metal and dielectric materials. We find that conventional wisdom inherited from circuit theory at radio and microwave frequencies does not usually obtain in the optical domain, and a true understanding of "plasmonic wave guiding" in this regime requires careful consideration of these properties.

We first review previous approaches to this problem by Brillouin [14], Landau [15], Loudon [16], and Ruppin [17] and then extend the Brillouin approach to a lossy, dispersive metal, carrying out an example calculation on the important conductor silver interfacing with air.

2. Electromagnetic Energy Density Calculations

2.A. The Poynting Vector

An expression for the energy density associated with electromagnetic vector fields occupying a volume including free space and material may be adduced from the two curl equations of Maxwell,

$$\boldsymbol{\nabla} \times \mathbf{E} + \frac{\partial \mathbf{B}}{\partial t} = 0 \tag{1}$$

$$\boldsymbol{\nabla} \times \mathbf{H} - \frac{\partial \mathbf{D}}{\partial t} = \mathbf{J} \tag{2}$$

where Eq. 1 is the Faraday-Law relation between electric field $\mathbf{E}$ and magnetic induction field $\mathbf{B}$ while Eq. 2 shows Ampère's Law relating the magnetic field $\mathbf{H}$, displacement field $\mathbf{D}$, and current density $\mathbf{J}$. A standard text book development [18] leads to

$$\boldsymbol{\nabla} \cdot (\mathbf{E} \times \mathbf{H}) + \mathbf{E} \cdot \mathbf{J} = -\mathbf{E} \cdot \frac{\partial \mathbf{D}}{\partial t} - \mathbf{H} \cdot \frac{\partial \mathbf{B}}{\partial t} \tag{3}$$

The right side of Eq. 3 clearly reflects the time rate of decreasing energy density; but in order to achieve a more geometrical interpretation of the left side of Eq. 3, we integrate both sides over the considered spatial volume and use the divergence theorem to convert volume integration of the first term on the left to a surface integral.

$$\begin{aligned} \int_S (\mathbf{E} \times \mathbf{H}) \cdot \mathbf{n}\, dA = &- \int_V \mathbf{E} \cdot \mathbf{J}\, dV \\ &- \int_V \left(\mathbf{E} \cdot \frac{\partial \mathbf{D}}{\partial t} + \mathbf{H} \cdot \frac{\partial \mathbf{B}}{\partial t} \right) dV \end{aligned} \tag{4}$$

It is clear that the the second term on the right side Eq. 4 represents the rate of decrease of field energy contained in the volume. The first term on the right is a volume integral over the scalar product of the E-field and current density within the volume. If we assume no current sources within the volume, the E-field can be written in terms of the current density and the material conductivity σ as $\sigma\mathbf{E} = \mathbf{J}$. The integrand of the first term on the right side of Eq. 4 is then written as J^2/σ and interpreted as the dissipative "Joule heating" or "ohmic

loss" within the volume. The term on the left therefore expresses the *total* decrease in energy density (radiative and dissipative). According to Poynting's theorem this term represents the flow of electromagnetic energy through the surface S enclosing the volume V. The vector product of $\mathbf{E}$ and $\mathbf{H}$ is termed the Poynting vector $\mathbf{S}$ and we write

$$\int_S \mathbf{S} \cdot \mathbf{n}\, dA = -\int_V \frac{\partial u}{\partial t}\, dV \tag{5}$$

where u is the total decrease of energy density–ohmic losses when they are present as well as loss from the radiating field itself. In free space or in nonconducting dielectric media we have

$$\begin{aligned}\int_S (\mathbf{E} \times \mathbf{H}) \cdot \mathbf{n}\, dA &= \int_S \mathbf{S} \cdot \mathbf{n}\, dA \\ &= -\int_V \left(\mathbf{E} \cdot \frac{\partial \mathbf{D}}{\partial t} + \mathbf{H} \cdot \frac{\partial \mathbf{B}}{\partial t} \right) \\ &= -\int_V \frac{\partial u}{\partial t}\, dV \end{aligned} \tag{6}$$

or in differential form

$$\boldsymbol{\nabla} \cdot \mathbf{S} = -\left(\mathbf{E} \cdot \frac{\partial \mathbf{D}}{\partial t} + \mathbf{H} \cdot \frac{\partial \mathbf{B}}{\partial t} \right) = -\frac{\partial u}{\partial t} \tag{7}$$

We are usually interested in the absolute value of the energy flow across the bounding surface; and, for harmonically oscillating waves, the average over an optical cycle. We have then,

$$\langle \mathbf{S} \rangle = \frac{1}{2} \Re \left(\mathbf{E} \times \mathbf{H}^* \right) \tag{8}$$

and

$$\begin{aligned}\langle \boldsymbol{\nabla} \cdot \mathbf{S} \rangle &= \\ &= \frac{1}{4} \left[\mathbf{E} \cdot \frac{\partial \mathbf{D}^*}{\partial t} + \mathbf{H} \cdot \frac{\partial \mathbf{B}^*}{\partial t} \right] = \left\langle \frac{\partial u}{\partial t} \right\rangle \end{aligned} \tag{9}$$

Equation 9, the optical-cycle average of the time rate of change of the energy density, is the starting point for our discussion of the energy density in material media subject to harmonic electromagnetic fields with frequencies covering the range from near-UV to near-IR spectral region.

The energy density, averaged over an optical cycle, of an electromagnetic field oscillating at frequency ω in a nonmagnetic material media characterized by permittivity $\epsilon = \epsilon_0 \epsilon_r$ and permeability μ_0 is given by

$$\begin{aligned} < u > &= \frac{1}{4} \left[\mathbf{E} \cdot \mathbf{D}^* + \mathbf{H} \cdot \mathbf{B}^* \right] \\ &= \frac{1}{4} \left[\epsilon(\omega) |\mathbf{E}^2| + \mu_0 |\mathbf{H}^2| \right] \end{aligned}$$

and with

$$|\mathbf{H}| = \sqrt{\frac{\epsilon(\omega)}{\mu_0}}|\mathbf{E}| \tag{10}$$

we have

$$< u >= \frac{1}{2}\epsilon(\omega)|\mathbf{E}|^2 = \frac{1}{2}\mathbf{E}\cdot\mathbf{D}^* \tag{11}$$

The relative permittivity ϵ_r (dielectric constant) may be complex with a real part ϵ_r' and an imaginary part ϵ_r''. The total *power density*, Eq. 9, with the help of Eq. 10, can now be written

$$< W(t) >= \left\langle \frac{\partial u}{\partial t} \right\rangle = \frac{1}{2}\left[\frac{1}{2}\left(\mathbf{E}+\mathbf{E}^*\right)\cdot\frac{1}{2}\left(\frac{\partial \mathbf{D}}{\partial t}+\frac{\partial \mathbf{D}*}{\partial t}\right)\right] \tag{12}$$

2.B. Brillouin Approach

Brillouin's analysis [14] of the energy density in lossless ($\epsilon_r = \epsilon'$), nonmagnetic material media starts from the careful statement that the *adiabatic* average energy density is given by the simple formula of Eq. 11. By "adiabatic" is meant that the field amplitude within the medium grows slowly from zero and varies over a time very long compared to the internal motions of the electron and nuclei of the material. To construct an adiabatically varying amplitude, as shown in Fig. 1, Brillouin establishes a composite field consisting of two "signal" frequencies ω_1, ω_2 symmetrically placed about a "carrier" ω,

$$\omega_1 = \omega + \nu$$
$$\omega_2 = \omega - \nu$$

The resulting electric field and its complex conjugate are then expressed as

$$\begin{aligned}\mathbf{E} &= \frac{1}{2}\mathbf{E}_0\left(e^{-i\omega_1 t} - e^{-i\omega_2 t}\right)\\ \mathbf{E}^* &= \frac{1}{2}\mathbf{E}_0\left(e^{i\omega_1 t} - e^{i\omega_2 t}\right)\end{aligned} \tag{13}$$

Using Brillouin's composite field, we seek to calculate the rate of change of the energy density by applying Eq. 12. The real part of the E-field can then be written as

$$\begin{aligned}\frac{1}{2}\left(\mathbf{E}+\mathbf{E}^*\right) &= \frac{1}{2}\mathbf{E}_0\left[\cos(\omega_1 t) - \cos(\omega_2 t)\right]\\ &= -\mathbf{E}_0\left[\sin(\omega t)\sin(\nu t)\right]\end{aligned}$$

Similarly the displacement fields $\mathbf{D}, \mathbf{D}^*$ can be written

$$\begin{aligned}\mathbf{D} &= \frac{1}{2}\epsilon_0\mathbf{E}_0\left[\epsilon_r(\omega_1)e^{-i\omega_1 t} - \epsilon_r(\omega_2)e^{-i\omega_2 t}\right]\\ \mathbf{D}^* &= \frac{1}{2}\epsilon_0\mathbf{E}_0\left[\epsilon_r^*(\omega_1)e^{i\omega_1 t} - \epsilon_r^*(\omega_2)e^{i\omega_2 t}\right]\end{aligned}$$

and after taking the time derivative of the displacement field, we have after extensive and somewhat tedious algebra an expression for the total energy density, including both electric and magnetic field contributions, in the ponderable medium.

$$\begin{aligned}\langle u\rangle &= \frac{1}{2}\epsilon_0|\mathbf{E}_0|^2\left[\frac{\partial\omega\epsilon_r'(\omega)}{\partial\omega}\right] \\ &= \frac{1}{2}\epsilon_0|\mathbf{E}_0|^2\left[\epsilon_r'(\omega)+\omega\frac{\partial\epsilon_r'(\omega)}{\partial\omega}\right]\end{aligned} \tag{14}$$

2.C. Landau Approach

In the Landau treatment [15], the time-varying field is given by,

$$\mathbf{E}(t) = \mathbf{E}_0(t)e^{-i\omega t} \tag{15}$$

where it is assumed that $\mathbf{E}_0(t)$ is a smoothly and slowly varying function with respect to the period $2\pi/\omega$. The time-dependent amplitude can then be expanded in a Fourier series as

$$\mathbf{E}_0(t) = \sum_\eta \mathbf{E}_\eta e^{-i\eta t} \tag{16}$$

With $\eta \ll \omega$, only slowly varying terms are retained in the Fourier expansion, and the time derivative of the displacement field $\mathbf{D}$ can be written

$$\frac{\partial\mathbf{D}}{\partial t} = i\omega\epsilon(\omega)\mathbf{E} + \frac{d(\omega\epsilon)}{d\omega}\frac{\partial\mathbf{E}}{\partial t}e^{-i\omega t}$$

Neglecting the imaginary part of the permittivity and dropping the subscript in ω_0, the total harmonic-time-averaged energy density, the sum of the contributions from the electric and magnetic fields, is found to be

$$\begin{aligned}\langle u\rangle &= \frac{1}{2}\epsilon_0|\mathbf{E}_0|^2\left[\frac{\partial\omega\epsilon_r'(\omega)}{\partial\omega}\right] \\ &= \frac{1}{2}\epsilon_0|\mathbf{E}_0|^2\left[\epsilon_r'(\omega)+\omega\frac{\partial\epsilon_r'(\omega)}{\partial\omega}\right]\end{aligned} \tag{17}$$

which is identical to the Brillouin result, Eq. 14.

2.D. Loudon Approach

In contrast to Brillouin and Landau, Loudon [16] analyzed the energy density for a wave propagating through a dispersive and *dissipative* medium with a single resonant frequency. He limited his treatment to the common case of nonmagnetic materials where dissipation occurs only with the E-field contribution to the energy density. This analysis including magnetic materials was carried out by Ruppin [17]. The permittivity is considered complex, $\epsilon = \epsilon' + i\epsilon''$ but the permeability μ is set equal to μ_0. Dissipative media are characterized by a

complex index of refraction $n = \eta(\omega) + i\kappa$, and the usual definition of the wave group velocity, $d\omega/dk$, does not lend itself to interpretation as the rate of energy transport through a lossy material. The wave vector $k = k_0 n$ becomes complex, and near an absorptive resonance use of the real part of $d\omega/dk$ can result in a "group velocity" greater than the speed of light in vacuum. Loudon recasts the *energy velocity* within lossy media as the ratio of the Poynting vector (time rate of energy flow normal to a unit area) and the energy density. The essential objective of Ref. 16 therefore, is the proper expression of energy density in dissipative media, and the simplest model for dissipation is a damped harmonic oscillator with a single resonance frequency ω_0 and damping rate γ.

Loudon begins with the electromagnetic wave propagating in a ponderable medium with polarization $\mathbf{P}$. Using the harmonic oscillator model, the equation of motion of the polarization wave is given by

$$\frac{d^2\mathbf{P}}{dt^2} + \gamma\frac{d\mathbf{P}}{dt} + \omega_0^2\mathbf{P} = \omega_p^2\epsilon_0\mathbf{E} \tag{18}$$

where ω_0 is the resonance frequency, γ the damping frequency, and ω_p parameterizes the interaction strength between the dipole oscillators in the medium and the electric field. It corresponds essentially to the bulk plasma frequency of a lossy metal. The resonance frequency ω_0 arises from a restoring force (per unit mass) $\mathbf{F}/m = -k_0\mathbf{r}$ with $k_0 = \omega_0^2$. The total energy density u now comprises two terms: a *stored energy* term u_s and *dissipative energy* term u_d. Under conditions of near-resonant absorption Loudon obtains the time-harmonic average electric-field contribution to the total energy density,

$$\langle u\rangle = \frac{1}{4}\epsilon_0|\mathbf{E}_0|^2\left(\epsilon_r' + \frac{2\epsilon_r''\omega}{\gamma}\right) \tag{19}$$

We can express the real and imaginary parts of the dielectric constant in terms of the oscillator properties using a well-known text book result from classical electrodynamics.

$$\epsilon_r' = 1 + \frac{\omega_p^2\left(\omega_0^2 - \omega^2\right)}{\left(\omega_0^2 - \omega^2\right)^2 + (\gamma\omega)^2} \tag{20}$$

$$\epsilon_r'' = \frac{\gamma\omega_p^2\omega}{\left(\omega_0^2 - \omega^2\right)^2 + (\gamma\omega)^2} \tag{21}$$

As expected Eq. 21 shows that when $\gamma \to 0$, $\epsilon_r'' \to 0$ and the second term inside the parentheses on the right side of Eq. 19 becomes

$$\frac{2\epsilon_r''\omega}{\gamma} \to \frac{2\omega_p^2\omega^2}{\left(\omega_0^2 - \omega^2\right)^2} \tag{22}$$

But from Eq. 20

$$\lim_{\gamma\to 0}\frac{d\epsilon_r'}{d\omega} = \frac{2\omega\omega_p^2}{\left(\omega_0^2 - \omega^2\right)^2}$$

and therefore the limiting expression for Eq. 19 as $\gamma \to 0$ is,

$$\lim_{\gamma \to 0} \langle u \rangle = \langle u_s \rangle = \frac{1}{4}\epsilon_0 |\mathbf{E}_0|^2 \left(\epsilon_r' + \omega \frac{d\epsilon_r'}{d\omega} \right) \tag{23}$$

equivalent to the Brillouin (Eq. 14) and Landau (Eq. 17) formulas for the stored energy density. When the dissipation rate γ is not negligibly small, we see from Eq. 19 that the term including the dissipative energy density, averaged over an optical cycle, is

$$\langle u_d \rangle = \frac{1}{2}\epsilon_0 \left|\mathbf{E}_0\right|^2 \frac{\epsilon_r'' \omega}{\gamma} \tag{24}$$

It is worthwhile noting that as $\gamma \to 0$, the dissipated *power density*,

$$\left(\frac{\gamma \omega^2}{\epsilon_0 \omega_p^2} \right) |\mathbf{P}|^2 = (\epsilon_0 \epsilon_r'' \omega) |\mathbf{E}|^2$$

goes to zero as expected, but the dissipative *energy density* $\langle u_d \rangle$, identified with the second term on the right in Eq. 19, does not. Of course one could alternatively define an average dissipative energy density as the product of the cycle-averaged dissapative power density and the period of the cycle,

$$\bar{u}_d = \frac{1}{2}\epsilon_0 \epsilon_r'' |\mathbf{E_0}|^2$$

and clearly $\bar{u}_d$ vanishes as $\gamma, \epsilon_r'' \to 0$.

It is also worthwhile noting that the Brillouin and Loudon expressions for the energy density become equivalent not only in the limit $\gamma \to 0$, but also in the free-electron-gas (FEG) limit, $\omega_0 \to 0$, where the restoring force on the oscillating electrons goes to zero. This limit corresponds to the Drude model of metals [19]. In this limit, with $\omega\tau >> 1$, Eqs. 20, 21 become

$$\epsilon_r' \to 1 - \frac{\omega_p^2}{\omega^2} \tag{25}$$

$$\epsilon_r'' \to \frac{\gamma \omega_p^2}{\omega^3} \tag{26}$$

From these last two expressions

$$\frac{d\epsilon_r'}{d\omega} = \frac{2\omega_p^2}{\omega^3} \qquad \text{and} \qquad \omega \frac{d\epsilon_r'}{d\omega} = \frac{2\epsilon_r'' \omega}{\gamma} \tag{27}$$

and once again we see that Eq. 14 is equivalent to Eq. 19.

3. Extended Brillouin Approach

Here we extend the Brillouin calculation of the energy density to include materials with loss. Since real metals are always somewhat lossy, and they figure importantly in the physics of

surface plasmon waves at optical frequencies, an expression for the energy density including loss has practical pertinence. We apply this approach to silver because its dispersion and loss can be well characterized as a single damped resonator. We expect therefore to obtain results similar to those obtained from Loudon's formula (Eq. 19)based on a single, damped harmonic oscillator. In subsequent work we will apply the extended-Brillouin method to other metals such as gold and aluminum where the optical response cannot be characterized so easily.

Starting with the Brillouin two-wave construction and writing out the *power* density, $W(t) = u/T$ with $T = 2\pi/\nu$, in terms of sines and cosines, we have

$$\begin{aligned}\langle W(t)\rangle = &\left[\frac{\epsilon_0|\mathbf{E}_0|^2}{4}\frac{\nu}{2\pi}\right]\times \\ &\left[2\nu\frac{\partial[\omega\epsilon'(\omega)]}{\partial\omega}\int_0^{2\pi/\nu}\left[\sin^2(\omega t)\sin(2\nu t)\right]dt\right. \\ &+4\omega\epsilon''(\omega)\int_0^{2\pi/\nu}\left[\sin^2(\omega t)\sin^2(\nu t)\right]dt \\ &+2\omega\epsilon'(\omega)\int_0^{2\pi/\nu}\left[\sin(2\omega t)\sin^2(\nu t)\right]dt \\ &\left.-\nu\frac{\partial[\omega\epsilon''(\omega)]}{\partial\omega}\int_0^{2\pi/\nu}\left[\sin(2\omega t)\sin(2\nu t)\right]dt\right] \end{aligned} \tag{28}$$

Figure 2 shows the electric field of the Brillouin wave, Eq. 13, as function of time for $\omega = 3\times10^{15}$ Hz and $\nu = 1\times10^{14}$ Hz. The figure also shows the slowly varying envelope $\sin(\nu t)$ to highlight the field amplitude slowly changing in time. Equation 28 can be written in terms of the integrals J_{1-4} as,

$$\begin{aligned}\langle W(t)\rangle = &\left[\frac{\epsilon_0|\mathbf{E}_0|^2}{4}\frac{\nu}{2\pi}\right]\times \\ &\left[2\nu\frac{\partial[\omega\epsilon'(\omega)]}{\partial\omega}J_1\left(\frac{2\pi}{\nu}\right)+4\omega\epsilon''(\omega)J_2\left(\frac{2\pi}{\nu}\right)\right. \\ &\left.+2\omega\epsilon'(\omega)J_3\left(\frac{2\pi}{\nu}\right)-\nu\frac{\partial\left[\epsilon''(\omega)\right]}{\partial\omega}J_4\left(\frac{2\pi}{\nu}\right)\right] \end{aligned} \tag{29}$$

where

$$J_1(t) = \frac{1}{4\nu}\Bigg[1 - \cos(2\nu t) + \frac{\nu^2\left(1 - \cos(2\omega t)\cos(2\nu t)\right) - \nu\omega\sin(2\omega t)\sin(2\nu t)}{(\omega^2 - \nu^2)}\Bigg]_0^t$$

$$J_2(t) = \frac{1}{4}\Bigg[t - \frac{\sin(2\omega t)}{2\omega} - \frac{\sin(2\nu t)}{2\nu} + \frac{\omega\sin(2\omega t)\cos(2\nu t) - \nu\cos(2\omega t)\cos(2\nu t)}{2\left(\omega^2 - \nu^2\right)}\Bigg]_0^t$$

$$J_3(t) = \frac{1}{4\omega}\Bigg[1 - \cos(2\omega t) - \frac{\omega^2\left(1 - \cos(2\omega t)\cos(2\nu t)\right) - \nu\omega\sin(2\omega t)\sin(2\nu t)}{(\omega^2 - \nu^2)}\Bigg]_0^t$$

$$J_4(t) = \frac{1}{2\nu}\left[\frac{\nu^2\sin(2\omega t)\cos(2\nu t) - \omega\nu\cos(2\omega t)\cos(2\nu t)}{(\omega^2 - \nu^2)}\right]_0^t$$

As is evident from inspection of Fig. 3, we are interested in the evaluation of the J functions at the four quadrant positions, $\pi/2\nu, \pi/\nu, 3\pi/2\nu, 2\pi/\nu$; and it is clear from the above expressions for J_{1-4} that, *averaged over the optical cycle of the slowly varying envelope*, the only nonvanishing integral is J_2, the term that represents dissipation. However, J_1 represents the transfer of energy between the electromagnetic field and the ponderable medium characterized by $\epsilon = \epsilon' + i\epsilon''$. This transfer is analogous to the energy oscillating from a driving source to passive capacitive and inductive elements in an electrical circuit [20]. It is common in electrical engineering to label this oscillating term as the "stored energy." The frequency of this transfer is twice the full optical cycle of the slowly varying envelope defined by $\nu = (\omega_1 - \omega_2)/2$. We are interested in the J_1 energy averaged over the *transfer* cycle; and therefore the appropriate limits of integration for this integral are from 0 to $\pi/2\nu$. Taking these limits we find the following expression for J_{1-4},

$$J_1\left(\frac{\pi}{2\nu}\right) = \frac{1}{2\nu} + \frac{\nu\cos^2(\omega\pi/2\nu)}{2\left(\omega^2 - \nu^2\right)}$$

$$J_2\left(\frac{\pi}{2\nu}\right) = \frac{1}{4}\left[\frac{\pi}{2\nu} - \frac{1}{2\omega}\sin(\omega\pi/\nu) - \left(\frac{\omega}{2\left(\omega^2 - \nu^2\right)}\right)\times\sin(\omega\pi/\nu)\right]$$

$$J_3\left(\frac{\pi}{2\nu}\right) = \frac{1}{2}\left[\frac{\sin^2(\omega\pi/2\nu)}{\omega} - \left(\frac{\omega}{\omega^2 - \nu^2}\right)\cos^2(\omega\pi/2\nu)\right]$$

$$J_4\left(\frac{\pi}{2\nu}\right) = -\frac{1}{2}\frac{\nu\sin(\omega\pi/\nu)}{\omega^2 - \nu^2}$$

The limiting expressions for these $J(t)$ functions at the quadrants of interest when $\omega \gg \nu$ are

$$J_1\left(\frac{\pi}{2\nu}\right) \to \frac{1}{2\nu}$$
$$J_2\left(\frac{\pi}{2\nu}\right) \to \frac{\pi}{8\nu}$$
$$J_3\left(\frac{2\pi}{\nu}\right) \to 0$$
$$J_4\left(\frac{2\pi}{\nu}\right) \to 0$$

and of course the average *energy* density is related to the average *power density* by

$$\langle u(t)\rangle = \langle W(t)\rangle\, T = \langle W(t)\rangle \left(\frac{2\pi}{\nu}\right) \tag{30}$$

Figure 3 shows the graphs of the kernels of the four J integrals for $\omega = 3 \times 10^{15}$ Hz and $\nu = 1 \times 10^{14}$ Hz. These plots immediately reveal some interesting physical aspects. The plot of the kernel of $J_1(t)$, panel (a) in Fig. 3, shows the same behavior as the term found in the lossless Brillouin and Landau treatments, while the kernel of $J_2(t)$, Fig. 3b, represents dissipation when loss is included. For the lossless, "stored energy" component the alternation in sign over the optical cycle can be interpreted as the energy oscillation between the field and the medium . The kernel of $J_2(t)$ shows, however, that dissipation does not change sign and takes place during both halves of the cycle. In order to find a general expression for the energy density, the expression in Eq. 28 must be integrated to time, t, and the energy density can be written in terms of these four integrals. Figure 4 shows the time evolution of the functions $J_{1-4}(t)$ that determine the time behavior of the E-field energy density terms of Eq. 28. It is clear from Fig. 4 a that this term describes alternating transfer between kinetic and potential energy of the harmonically oscillating electron. In Figs. 4 c and 4d the rapidly oscillating terms integrate to zero even for a quarter period. Quite different behavior, however, obtains for Fig.4 b. This integral represents dissipated energy density in the medium that grows with time and never returns to the field. The first term of Eq. 29 represents the power exchanged between the medium and the E-field at each quarter of the oscillation period and corresponds to an average stored energy density,

$$\langle u_s\rangle = \frac{\epsilon_0 \left|\mathbf{E}_0\right|^2}{4}\left[\frac{\partial[\omega\epsilon_r'(\omega)]}{\partial\omega}\right] \tag{31}$$

while the second term represents the energy dissipated by the lossy medium in an optical period.

$$\langle u_d\rangle = \frac{1}{4}\epsilon_0 \left|\mathbf{E}_0\right|^2 \omega\epsilon_r''(\omega)\left(\frac{2\pi}{\nu}\right) \tag{32}$$

For a lossless medium ϵ'' vanishes and the original Brillouin expression, Eq. 14 is recovered. In the free-electron-gas limit, from Eq. 26, we have

$$\langle u_d \rangle = \frac{1}{4}\epsilon_0 \left|\mathbf{E}_0\right|^2 \frac{\gamma\omega_p^2}{\omega^2}\left(\frac{2\pi}{\nu}\right) \tag{33}$$

Comparing the Loudon expression for the dissipated energy density, Eq. 24, to that of the Extended Brillouin, Eq. 32, we find that they differ in two respects: first, the factor $1/\gamma$ in the Loudon expression represents the rate of "collisional" or "radiative" dissipation while the factor $2\pi/\nu$ in Eq. 32 represents the bandwidth of the slowly varying envelope, $\nu = (\omega_1 - \omega_2)/2$. Second, the Brillouin dissipation energy is essentially 1/2 that of the Loudon result. The additional factor of 1/2 arises from the rapid modulation of the "signal" wave ν by the "carrier" wave ω. Figure 5 shows these relationships.

4. Application to Silver

We apply the energy density expressions obtained by the Loudon (Eq. 19), using the expressions for ϵ' and ϵ'' in the FEG limt (Eqs. 25, 26), and Extended Brillouin (Eqs. 31, 32) approaches to the specific case of silver metal. The application takes place in two steps: the first is to obtain differentiable analytic fits to the dispersive permittivity of the material, and the second is to substitute them into Eq. 19 and Eqs. 31, 32.

Measurements of the wavelength dependence of the real and imaginary parts of the silver permittivity have been compiled from various sources and tabulated by Palik [21]. A second data set are the measurements reported by Johnson and Christy [22]. In Fig. 6 we plot (filled circles) the Palik permittivity data for ϵ' (panel A) and ϵ'' (panel B).

The plots of ϵ' and ϵ'' vs. wavelength clearly show two branches above $\lambda = 1200\,\text{nm}$. We consider these data as two different sets, a lower branch and an upper branch. The lower branch in ϵ' corresponds to the upper branch in ϵ''. We obtain analytic fits in two ways: first using the dispersion relations of the harmonic oscillator (HOM) in the FEG limit, Eqs. 25, 26 and second by applying a polynomial fitting procedure to the data points. In both cases we have used the lower-branch points in Fig. 6 A. For the harmonic oscillator model we first fit Eq. 25 to the ϵ' curve to obtain a value for ω_p which was then substituted into Eq. 26 to obtain γ. The resulting fits for ϵ' in Fig. 6 A and ϵ'' in Fig. 6 B are shown by the thick dashed lines. The HOM FEG model fits the Ag permittivity dispersion quite well which shows that silver is well-characterized as a simple Drude metal. The data were also fit using a quadratic spline for $\epsilon'(\lambda)$ and cubic spline for $\epsilon''(\lambda)$. The polynomial fits are indicated by the solid line in Figs. 6 A,B.

In Fig. 7 we plot the Johnson-Christy data set for ϵ' and ϵ'', using the same procedures. For both data sets excellent fits are obtained although ω_p and γ determined from the HOM

fitting are not the same between the two data sets. Note that the values of ϵ'' for the Palik data set are about a factor of two higher than those in the Johnson-Christy data set.

5. Discussion

In Figs. 8, 9 are plotted the stored and dissipative energy densities for Ag as a function of wavelength (normalized to $\epsilon_0 E_0^2$), using the Palik and Johnson-Christy data, respectively. From both data sets it is quite clear that the HOM FEG model reproduces quite well the energy density of Ag metal over a wavelength range from about 600 nm to 1700 nm. The deviations in $u_d(\lambda)$ at lower end of the wavelength scale, near 400 nm, is due to the absorptive plasmon resonance—evident in panel (B) of Figs. 6, 7. Since the optical response of Ag is essentially that of a free-electron gas, calculation of the energy densities with Eqs. 31, 32, the Extended Brillouin expressions, produces very similar results. For other metals such as gold or aluminum, the dispersion of the real and imaginary parts of the permittivity cannot be characterized so easily. We will show in a subsequent report that in these cases, where the HOM FEG model fails, the dispersion of the real and imaginary parts of the permittivity can still be well fit to a polynomials and energy density calculated with the Extended Brillouin expressions.

References

1. V. Giannini, A. Berrier, S. M. Maier, J. A. Sanchez-Gil, and J. G. Rivas, "Scattering efficiency and near field enhancement of active semiconductor plasmonic antennas at terahertz frequencies," Opt. Express **18**, 2797–2807 (2010).
2. M. Mansuripur, A. R. Zakharian, A. Lesuffleur, S. H. Oh, R. J. Jones, N. C. Lindquist, H. Im, A. Kobyakov, and J. V. Moloney, "Plasmonic nano-structures for optical data storage," Opt. Express **17**, 14001–14014 (2009).
3. S. Sederberg, V. Van, and A. Y. Elezzabi, "Monolithic integration of plasmonic waveguides into a complimentary metal-oxide-semiconductor- and photonic-compatible platform," Appl. Phys. Lett. **96**, 121101 (2010).
4. N. C. Lindquist, W. A. Luhman, S. H. Oh, and R. J. Holmes, "Plasmonic nanocavity arrays for enhanced efficiency in organic photovoltaic cells," Appl. Phys. Lett. **93**, 123308 (2008).
5. N. Engheta, "Circuits with light at nanoscales: Optical nanocircuits inspired by metamaterials," Science **317**, 1698–1702 (2007).
6. H. S. Chen, L. X. Ran, J. T. Huangfu, T. M. Grzegorczyk, and J. A. Kong, "Equivalent circuit model for left-handed metamaterials," J. Appl. Phys. **100**, 024915 (2006).
7. H. J. Lezec, J. A. Dionne, and H. A. Atwater, "Negative refraction at visible frequencies," Science **316**, 430–432 (2007).
8. P. G. Luan, "Power loss and electromagnetic energy density in a dispersive metamaterial medium," Phys. Rev. E **80**, 046601 (2009).
9. A. D. Boardman and K. Marinov, "Electromagnetic energy in a dispersive metamaterial," Phys. Rev. B **73**, 165110 (2006).
10. S. A. Tretyakov, "Electromagnetic field energy density in artificial microwave materials with strong dispersion and loss," Phys. Lett. A **343**, 231–237 (2005).
11. K. J. Webb and Shivanand, "Electromagnetic field energy in dispersive materials," J. Opt. Soc. Am. B **27**, 1215–1220 (2010).
12. J. A. Dionne, L. A. Sweatlock, H. A. Atwater, and A. Polman, "Plasmon slot waveguides: Towards chip-scale propagation with subwavelength-scale localization," Phys. Rev. B **73**, 035407 (2006).
13. E. Feigenbaum and H. A. Atwater, "Resonant guided wave networks," Phys. Rev. Lett. **104**, 147402 (2010).
14. L. Brillouin, *Group Velocity and Wave Propagation* (Academic Press, 1960).
15. L. D. Landau and E. M. Lifshitz, *Electrodynamics of Continuous Media* (Pergamon Press, 1984), 2nd ed.
16. R. Loudon, "Propagation of electromagnetic energy through an absorbing dielectric," J.

Phys. A: Gen. Phys. **3**, 233–245 (1970).

17. R. Ruppin, "Electromagnetic energy density in a dispersive and absorptive material," Phys. Lett. A **299**, 309–312 (2002).
18. D. Griffiths, *Introduction to Electrodynamics* (Prentice-Hall, 1999), third edition.
19. M. Born and E. Wolf, *Principles of Optics, sixth edition* (Pergamon Press, 1993), sixth edition.
20. J. W. Nilsson and S. Riedel, *Electric Circuits* (Prentice Hall, 2010), 9th ed.
21. E. Palik and G. Ghosh, eds., *The Electronic Handbook of Optical Constants of Solids* (Academic, New York, 1999).
22. P. B. Johnson and R. W. Christy, "Optical constants of noble metals," Phys. Rev. B **6**, 4370–4379 (1972).

Figure captions

Fig. 1

Brillouin composite field consisting of two "signal fields" with frequencies ω_1, ω_2 displaced symmetrically above and below the "carrier" at ω_0. Superposition produces a slowly varying envelope in which the amplitude of the rapidly varying carrier is modulated.

Fig.2

Solid line shows electric field behavior in time as expressed by Eq. 13. Dashed line shows slowly varying envelope.

Fig.3

Plots of the integrands for the four constituent J_n functions included in the power density expression, Eq. 29. J_{1-4} correspond to (a)-(d), respectively.

Fig.4

Time behavior of the integrals $J_{1-4}(t)$.

Fig.5

The "signal" sine wave $\sin^2 \nu t$ is rapidly modulated by the "carrier" sine wave $\sin \omega^2 t$ and can be replaced by the factor $1/2 \sin^2(\nu t)$. Averaging over the optical cycle period T results in the factor $1/4$ in Eq. 32.

Fig.6

(A) Plot of the Palik data [21] for ϵ' vs. wavelength is shown in filled circles. Fits to these data points are indicated for the FEG HOM model by thick dashed lines and for the polynomial fit by the solid line. (B) Similar plots of Palik data [21] for ϵ''.

Fig.7

(A) Plot of the Johnson and Christy data [22] for ϵ' vs. wavelength is shown in filled circles. Fits to these data points are indicated for the FEG HOM model by thick dashed lines and for the polynomial fit by the solid line. (B) Similar plots of Johnson and Christy data [22] for ϵ''.

Fig.8

Stored energy density (left panel) and dissipative energy denisty (right panel). Dashed curves traces the FEG HOM model (Eqs. 19,25, 26) normalized to $\epsilon_0 E_0^2$. Solid curve traces the Brillouin Extended expressions (Eqs. 31, 32) using fitted polynomials to the Palik data for ϵ' and ϵ''.

Fig.9

Stored energy density (left panel) and dissipative energy denisty (right panel). Dashed curves traces the FEG HOM model (Eqs. 19,25, 26) normalized to $\epsilon_0 E_0^2$. Solid curve traces the Brillouin Extended expressions (Eqs. 31, 32) using fitted polynomials to the Johnson-Christy data for ϵ' and ϵ''.

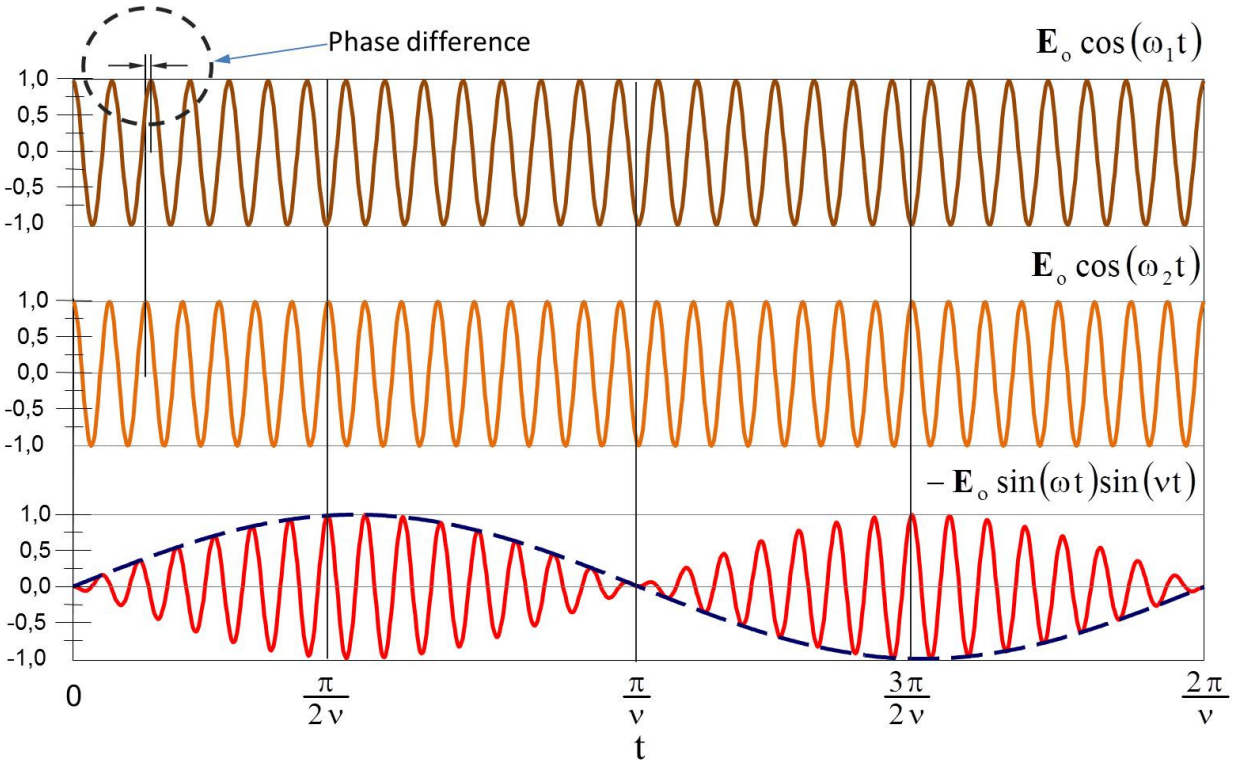

Fig. 1. Brillouin composite field consisting of two "signal fields" with frequencies ω_1, ω_2 displaced symmetrically above and below the "carrier" at ω_0. Superposition produces a slowly varying envelope in which the amplitude of the rapidly varying carrier is modulated.

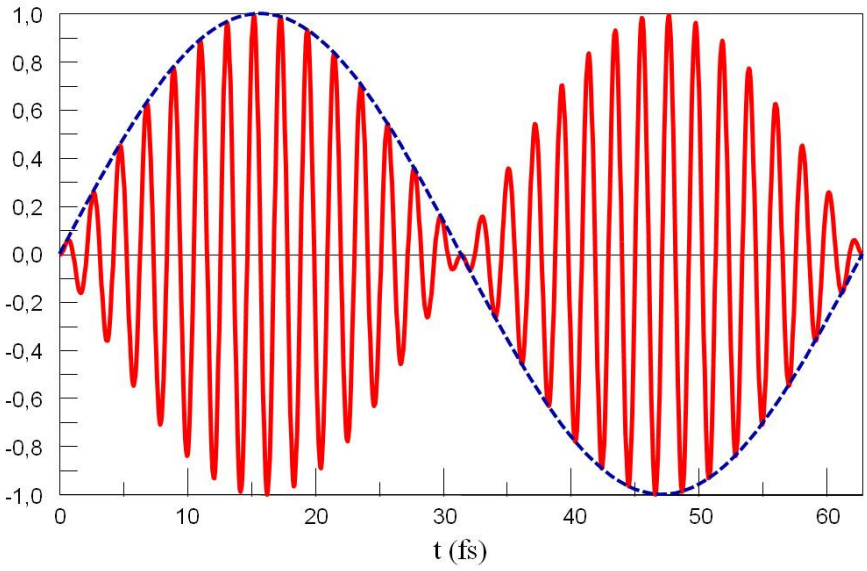

Fig. 2. Solid line shows electric field behavior in time as expressed by Eq. 13. Dashed line shows slowly varying envelope.

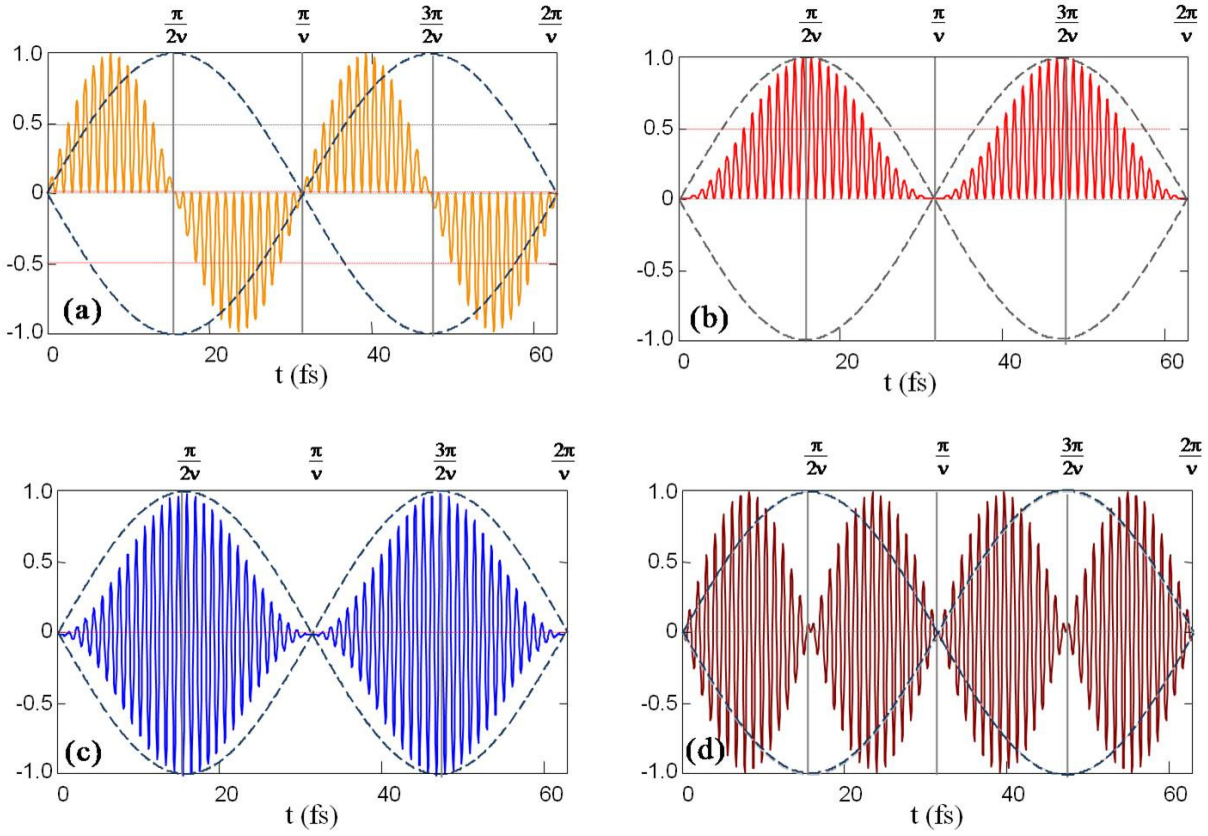

Fig. 3. Plots of the integrands for the four constituent J_n functions included in the power density expression, Eq. 29. J_{1-4} correspond to (a)-(d), respectively.

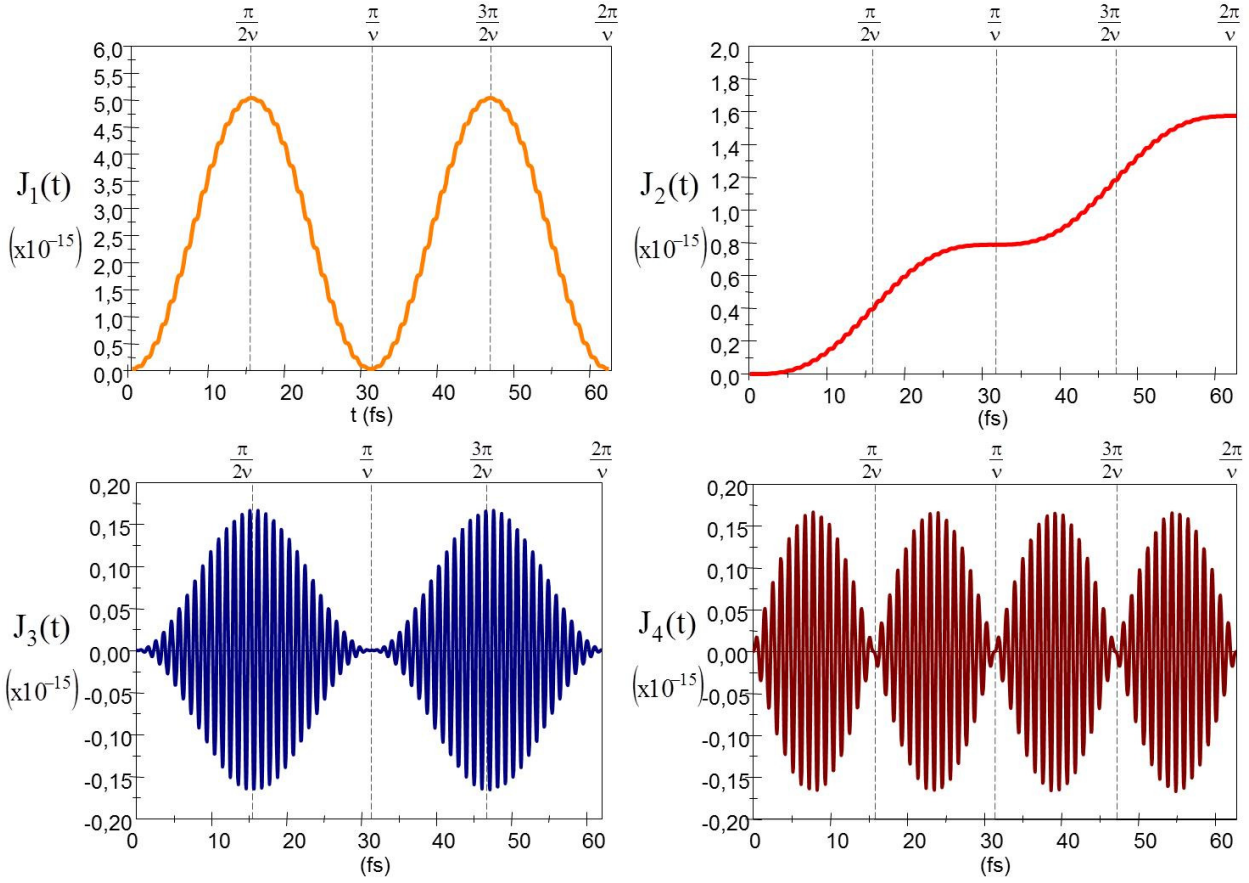

Fig. 4. Time behavior of the integrals $J_{1-4}(t)$.

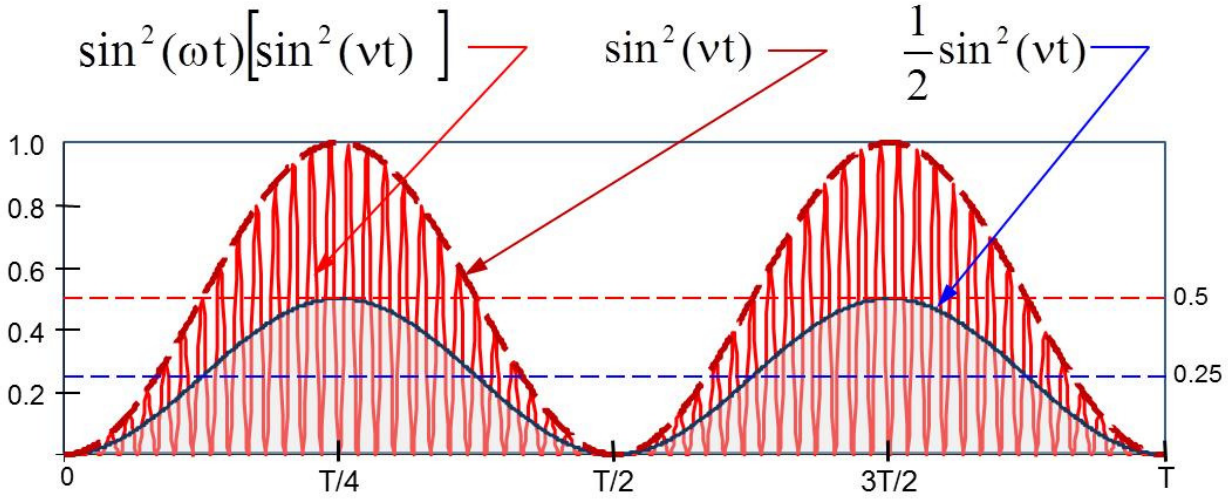

Fig. 5. The "signal" sine wave $\sin^2 \nu t$ is rapidly modulated by the "carrier" sine wave $\sin \omega^2 t$ and can be replaced by the factor $1/2 \sin^2(\nu t)$. Averaging over the optical cycle period T results in the factor $1/4$ in Eq. 32.

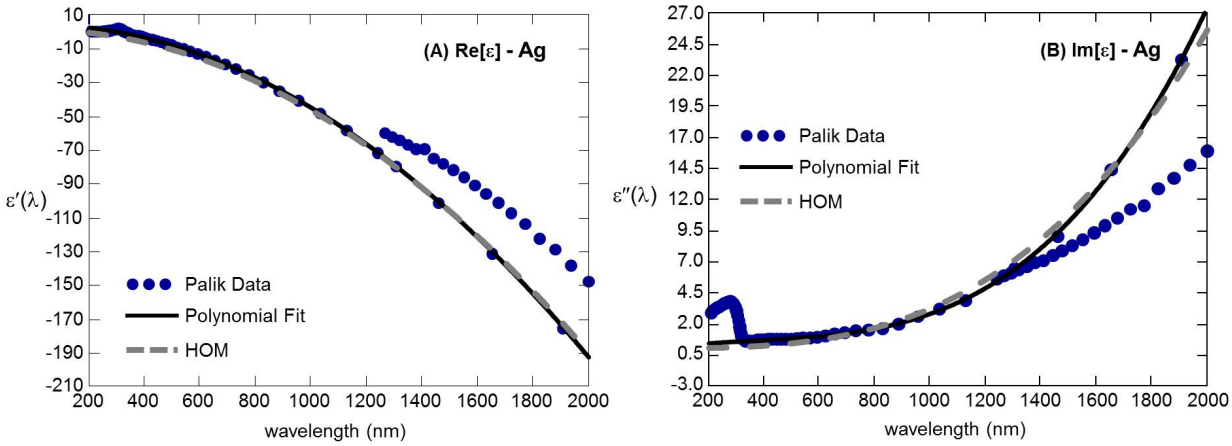

Fig. 6. (A) Plot of the Palik data [21] for ϵ' vs. wavelength is shown in filled circles. Fits to these data points are indicated for the FEG HOM model by thick dashed lines and for the polynomial fit by the solid line. (B) Similar plots of Palik data [21] for ϵ''.

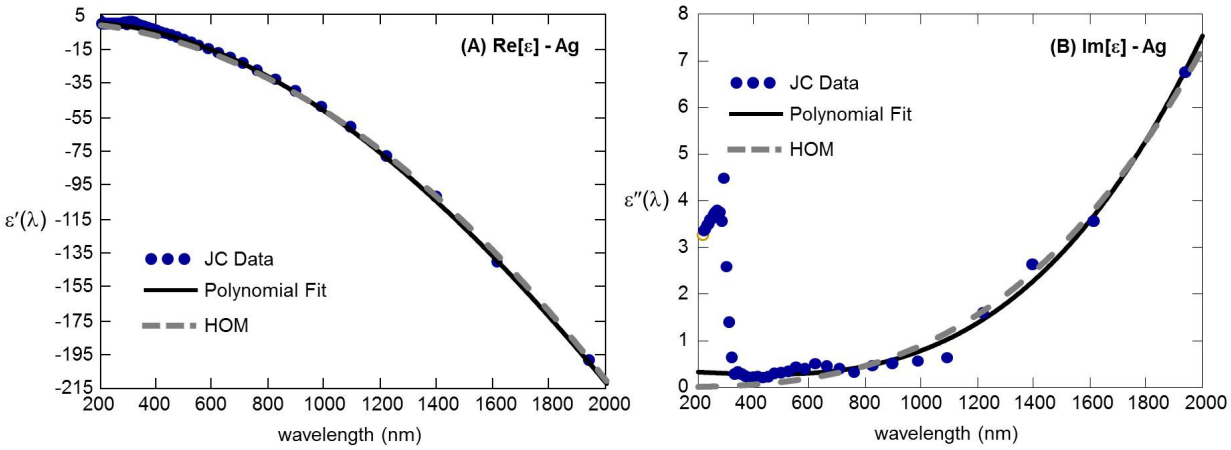

Fig. 7. (A) Plot of the Johnson and Christy data [22] for ϵ' vs. wavelength is shown in filled circles. Fits to these data points are indicated for the FEG HOM model by thick dashed lines and for the polynomial fit by the solid line. (B) Similar plots of Johnson and Christy data [22] for ϵ''.

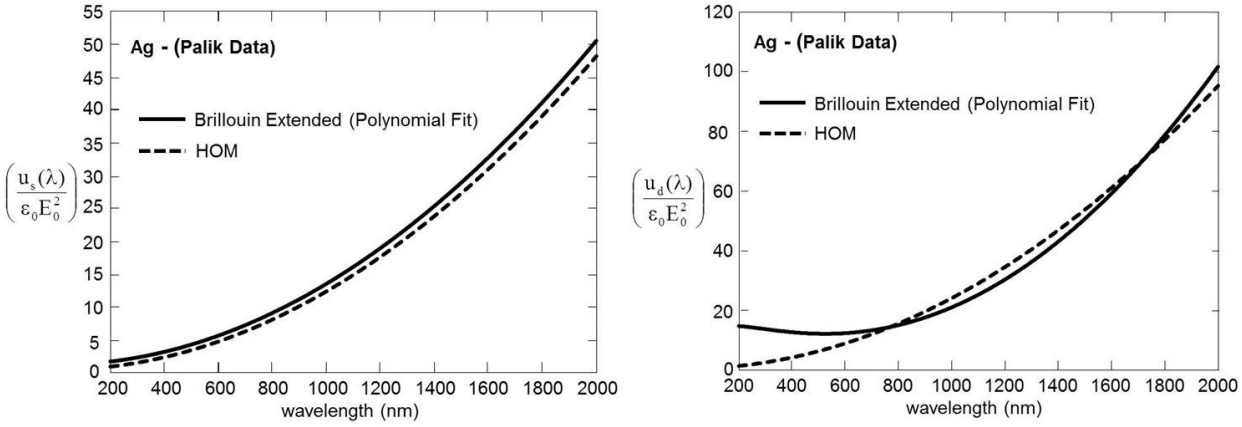

Fig. 8. Stored energy density (left panel) and dissipative energy denisty (right panel). Dashed curves traces the FEG HOM model (Eqs. 19,25, 26) normalized to $\epsilon_0 E_0^2$. Solid curve traces the Brillouin Extended expressions (Eqs. 31, 32) using fitted polynomials to the Palik data for ϵ' and ϵ''.

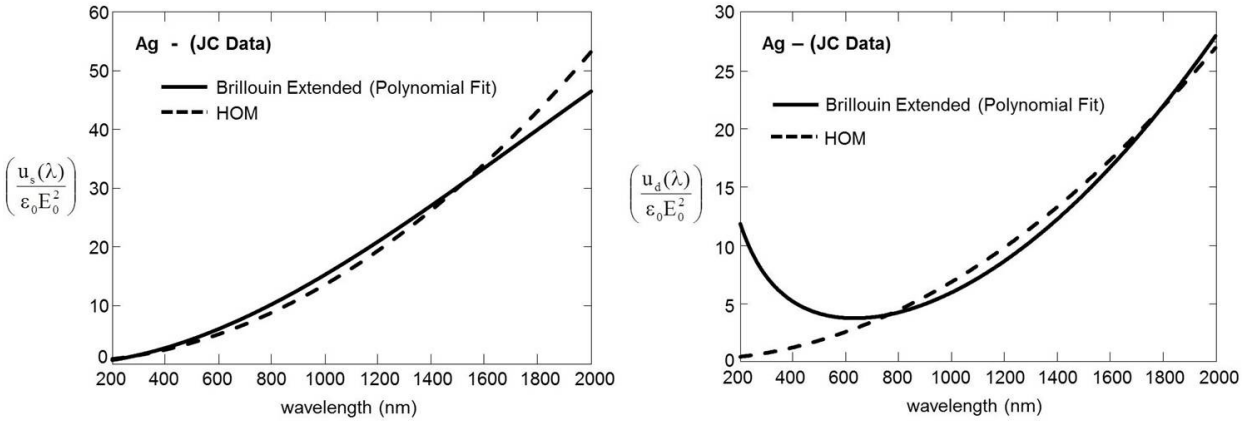

Fig. 9. Stored energy density (left panel) and dissipative energy denisty (right panel). Dashed curves traces the FEG HOM model (Eqs. 19,25, 26) normalized to $\epsilon_0 E_0^2$. Solid curve traces the Brillouin Extended expressions (Eqs. 31, 32) using fitted polynomials to the Johnson-Christy data for ϵ' and ϵ''.